

# Dynamic analysis of inverter dominated unbalanced LV micro-grids

N. L. Soutanis, A. I. Tsouchnikas, N. D. Hatziaargyriou, J. Mahseredjian

**Abstract—** This paper presents simulation of the dynamic behavior of low voltage micro-grids both under grid connected and autonomous operation. In LV micro-grids it is most likely that the sources participating in the system are connected to the network with inverters. This results in the formation of an inertia-less system. Modeling has to allow for the representation of all characteristic unbalances encountered in the LV network. The simulation is conducted using the electromagnetic transient analysis program EMTP-RV.

**Index Terms—** distributed generation (DG), micro-grids, inverter control, low voltage networks

## I. INTRODUCTION

DRIVING forces such as environmental concerns and the need for energy efficiency, tied with technical progress in new forms of energy production, favor the shift towards a decentralized power system. Distributed generators (DG) with prime sources based either on renewable energy or on natural gas are installed in distribution or higher voltage networks. A large scale integration of DGs is anticipated for lower voltage networks, promising distinct advantages for the consumers regarding reliability and power quality [1][2]. Low voltage feeders with several micro-sources [3][4], storage devices and controllable loads that appear to the upstream distribution network as a controllable entity, form the so called micro-grids [1][2]. The micro-grid can operate either connected with the MV distribution grid exchanging power with it according to the existing conditions or autonomously in the event of upstream network unavailability.

The micro-grid is an intensive application of distributed generation, therefore dynamic analysis is required to ensure that it operates in a stable manner and that voltage and frequency fluctuations are maintained within acceptable limits [1]-[3]. The isolation from the upstream grid and the subsequent autonomous operation are challenging. Proper load sharing among the micro-sources has to be ensured along with good dynamic response characteristics following any disturbance.

A LV micro-grid may be essentially an inertia-less system, since all sources may be connected to the network via inverters to gain in control flexibility or to bridge incompatibilities between the output of the sources and the network. In addition the special features of LV networks, such as uneven phase loading, the presence of single and three-phase lines have to be accounted for in the network representation. In this paper electromagnetic transient analysis program EMTP-RV [5] is used to examine the dynamics of the micro-grid. The EMTP-RV can be used to simulate the dynamics of any poly-phase system accurately. There is no limitation in the system topology and the lines can have any number of wires. The instantaneous values of voltages and currents can have any arbitrary form beyond the sinusoidal fundamental waveform and every system component is described by a set of differential equations. Frequency is a natural property of the system quantities and the inertia of rotating machines is not necessary for its computation. Moreover, the operation and control of the electronic converters can be modeled in detail [6]. EMTP-RV provides a steady state poly-phase load flow for the initialization of the state variables, so that the time domain simulation starts from a specified steady state condition avoiding unnecessary transients.

In [7] a stability algorithm for the dynamic analysis of inverter dominated micro-grids in island operation has been proposed and the simulation results have been verified by EMTP-RV. This paper focuses on the EMTP-RV application to the dynamic analysis of micro-grids and presents new data, simulation results and analysis.

## II. CHARACTERISTICS OF LV MICRO-GRIDS

Low voltage networks of urban and rural areas bear some distinct features that need to be accounted for in their analysis (steady state load flows, fault calculations or transient simulations). Unbalanced loading and excitation are very common and result from the uneven load distribution among the three phases and from the existence of single-phase sources. Moreover, the network structure itself may be unbalanced, mainly due to single-phase laterals or the inherent asymmetry of the three phase lines. Unlike high voltage networks, line impedances are predominantly resistive, while their shunt capacitance is typically ignored. Basically, the structure of the LV network differs from HV networks in that any LV line, in addition to the phase conductors, will also include a grounded or ungrounded neutral conductor and

---

This work was performed with the EU research project "Micro-grids" (Contract No ENK 5-CT-2002-00610). The authors gratefully acknowledge the support received from the European Union for this research.

N. L. Soutanis, A. I. Tsouchnikas and N. D. Hatziaargyriou are with the National Technical University of Athens, Athens, 15780 Greece (phone: 30-210-7723696; fax:30-210-7723968; e-mail: nsoutan@power.ece.ntua.gr / aggelos@power.ece.ntua.gr / nh@power.ece.ntua.gr).

Jean Mahseredjian is with École Polytechnique de Montréal.

possibly a separate protective earth (grounding) conductor. In public LV distribution networks the neutral is typically multi-grounded, at the source, consumer service points and possibly other selected locations along the lines. In such a case, a parallel return path exists through the earth for neutral (zero sequence) current, even in the absence of any fault. In unfaulted conditions, however, this return path is customarily ignored with negligible error, since the neutral conductor presents a much lower return impedance [8].

As far as the sources that participate in the system are concerned, they can be classified on the basis of their capability to produce controlled active power on demand.

Sources which lack this capability (such as photovoltaics or wind turbines) are normally operated under PQ control [2], ensuring that maximum active power  $P$  is extracted from the prime source, under a constant reactive power  $Q$  or power factor (possibly regulated). This control type remains the same, whether the system operates connected to the upstream network or not.

Sources based on storage devices or regulated prime movers, on the other hand, permit the controlled variation of their output power, within the limits set by the primary energy buffer and their rated capacity. Such sources are assigned the task of frequency regulation during autonomous operation of a micro-grid and are often described as “grid-forming units”, since they are responsible for setting up and regulating the network where the PQ-controlled sources are connected [9]. In the isolated mode of operation, the system load is fed only by the local micro-sources. Thus the grid forming units are called upon to regulate frequency and voltage for the loads and the PQ-controlled sources, a function in principle equivalent to maintaining the active and reactive power balance within the island system. Grid-forming units are interfaced to the network through voltage source inverters, whose frequency and voltage is regulated using “frequency – active power” and “voltage – reactive power” characteristics, emulating the droop curves of traditional generators [9]-[14]. This allows proper load sharing among multiple regulating units within the same network. This type of control is carried out only with local measurement of terminal quantities, without any communication requirements between individual units and can operate when the micro-grid is connected to the main grid as well.

The two control types discussed above are implemented in the inverter that interfaces the sources to the network. In particular, the control algorithms regulate the magnitude and phase angle of the inverter internal voltage (actually of the fundamental component of the respective PWM waveform). Hence in the case of storage units the frequency/angle is controlled by active power–frequency droop and the magnitude by reactive power–voltage droop as shown for the EMTP-RV implementation of control in Fig. 1. Two first order transfer functions with time constants  $T_m$  and  $T_e$  are used for the active and reactive power measurement delay respectively. The time constants can be also adjusted to decouple the active and reactive power control channels. The

phase angle derived by integrating the frequency and the magnitude resulting from the reactive power droop control constitute the desired internal emf voltage vector. The stabilizing factor is a gain with units rad/W which adds phase lead to the system and improves the response and stability especially in the case of network lines with high resistance to reactance ratio.

Sources operated under PQ control are considered to be connected to the network via voltage source inverters, as well. In this case, the angle and magnitude of the internal AC voltage are controlled in order to maintain the dc side voltage at a specified reference value and the reactive power output at a desired set point [15], as shown in Fig. 2.

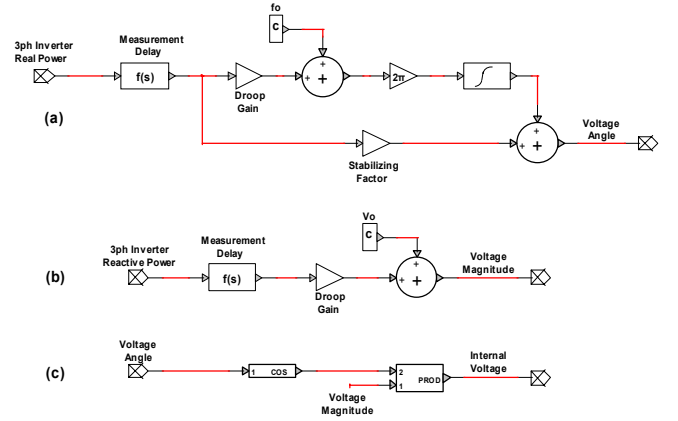


Fig. 1. Control of storage units and regulated sources via droop curves (one for frequency–active power and one for internal voltage–reactive power).  $V_0$ ,  $f_0$ , correspond to zero  $Q$ ,  $P$  output.

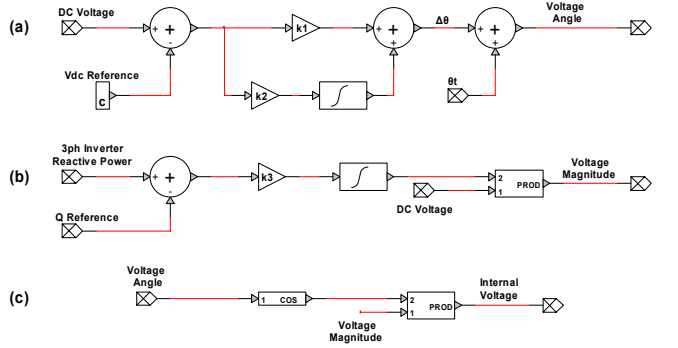


Fig. 2. PQ-type control (non regulated Microsources).

The power balance between the inverter output power and the power produced by the primary source determines the dc side voltage. The angle difference  $\Delta\theta$  between the inverter internal and terminal voltages is derived from the dc voltage error via a PI controller.  $\Delta\theta$  and the phase angle  $\theta_t$  of the terminal voltage yield the phase angle  $\theta = \theta_t + \Delta\theta$  of the internal emf. The deviation of the reactive power from its set-point yields the magnitude of the internal emf via an I-controller.

### III. APPLICATIONS

#### A. Test System

The study case LV micro-grid built in EMTP-RV is shown

in Fig. 3. Details can be found in [16]. Network data are provided in the Appendix. Two storage units are connected at nodes A and B, providing regulation in the isolated mode of operation. Both of them are battery banks coupled to the network through voltage source inverters, controlled as described in Fig. 1. Two PV units are connected at nodes C and D through inverters controlled as shown in Fig. 2. A wind turbine equipped with an induction generator directly coupled to the grid is connected at node E.

The rated capacities of the storage units at nodes A and B are respectively 35 kVA and 25 kVA, at p.f. 0.85 lag. Their droop curves are specified so that the units produce zero active and reactive power when the micro-grid is connected to the main grid. The slopes of the droop curves, given in the Appendix, determine the output power (generated or consumed) in relation to the micro-grid frequency and unit internal voltage. E.g. for the selected slopes of the P-f curves, the maximum output power of each unit corresponds to a frequency deviation of  $\pm 0.5$  Hz, while active and reactive power production is in proportion to their rating.

### B. Simulation results

Two cases were examined and selected graphs of the system quantities are presented.

In the first of the simulated cases, only the two battery units are in operation, all other sources being disconnected. The micro-grid is initially connected to the main grid, disconnecting at 1 sec. Then, the load at nodes C, D, and E increases by 25% at 2.5 sec. Node voltages, currents and power flows are plotted in Figs. 4 to 12.

Initially, the load is fed by the upstream network. The sum of the active power output of the three phases in each of the two battery inverters is zero (Figs. 7, 9), as dictated by the P-f droops for system frequency equal to 50 Hz (Fig. 4). At the same time, the internal voltages of the two inverters assume a value corresponding to zero total reactive power output (sum of three phases) (Figs. 5, 8, 10). On separation of the micro-grid from the main grid, at  $t=1$  sec, the power output of the storage units abruptly increases to meet the total load demand (Figs 6,7,9). This increase in active power results in a reduction of the micro-grid frequency (Fig. 4), as dictated by the P-f droop curves. Eventually, a new equilibrium point is established, where the two storage units operate at a lower system frequency, sharing the total micro-grid load in proportion to their rated capacities.

Reactive power demand from the two inverters also increases (Figs 6,8,10), to meet the load demand, resulting in increased internal voltages (Fig. 5), according to their Q-V droop curves. The voltage level throughout the network drops somewhat, but is kept at an acceptable level, as seen in Fig. 11 for the load node C. The active and reactive power demands of this load are shown in Fig. 12 and they remain practically unaffected.

At  $t=2.5$  s a 25% load increase at nodes C, D and E occurs, balanced by a further increase in the active and reactive power production of the two storage units (Figs. 6-10). The micro-

grid frequency drops further (Fig. 4), while the internal voltages of the inverters are increased (Fig. 5).

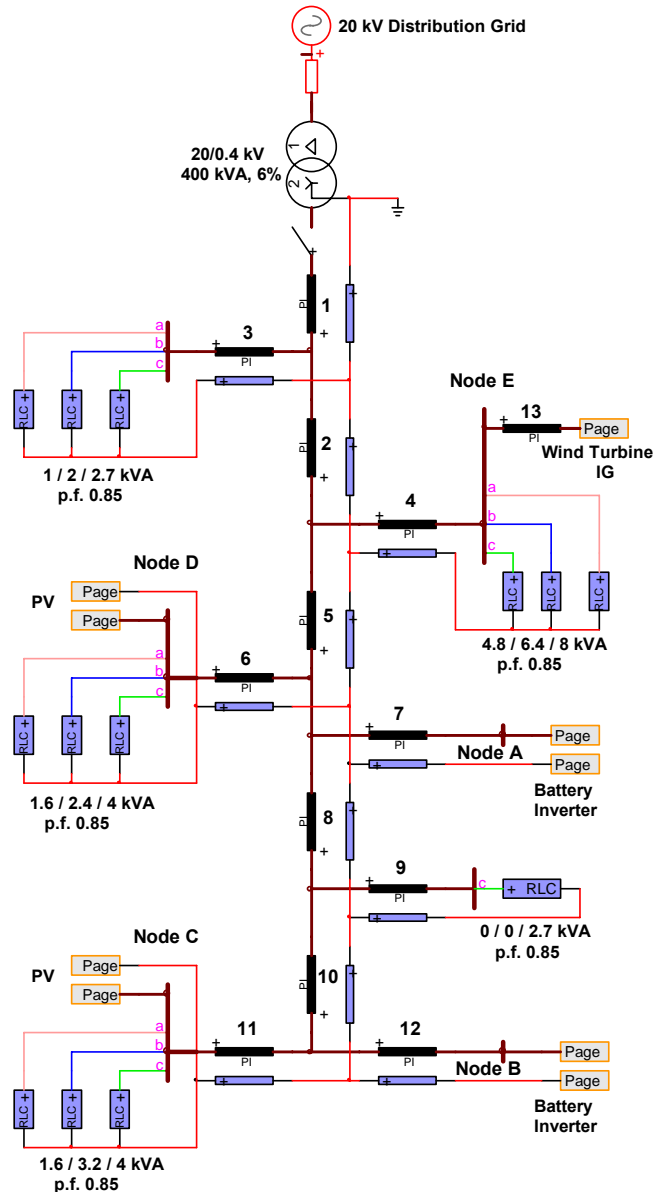


Fig. 3. The study case Micro-grid network.

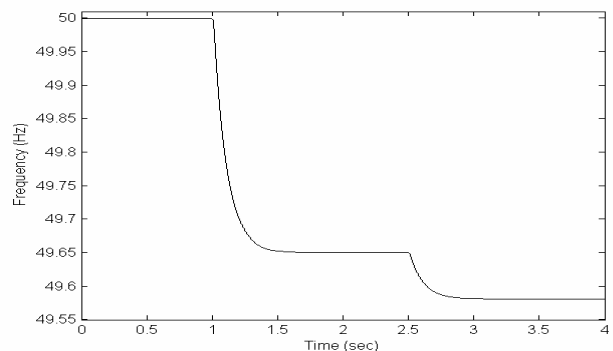


Fig. 4. Micro-grid frequency (measured at the terminals of the two battery units).

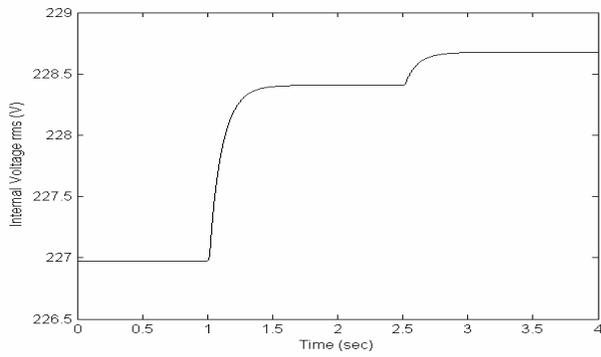


Fig. 5. Internal phase voltages of the battery inverter at node A.

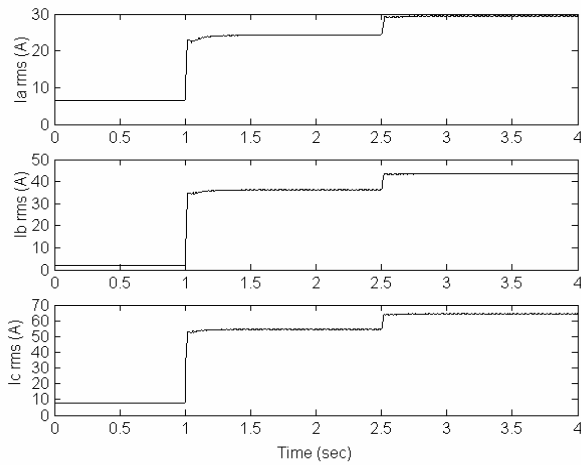


Fig. 6. Currents of the battery inverter at node A.

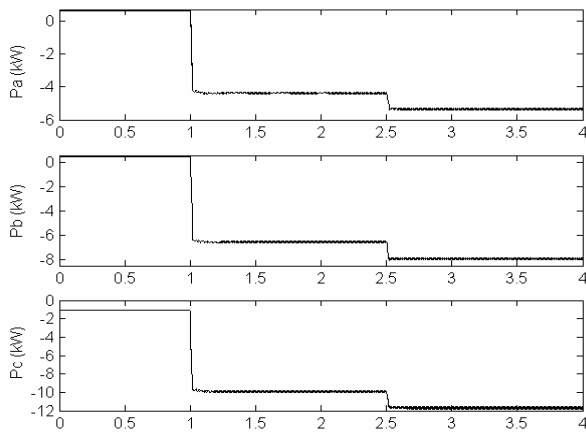


Fig. 7. Active power flow per phase, of the inverter at node A (load convention).

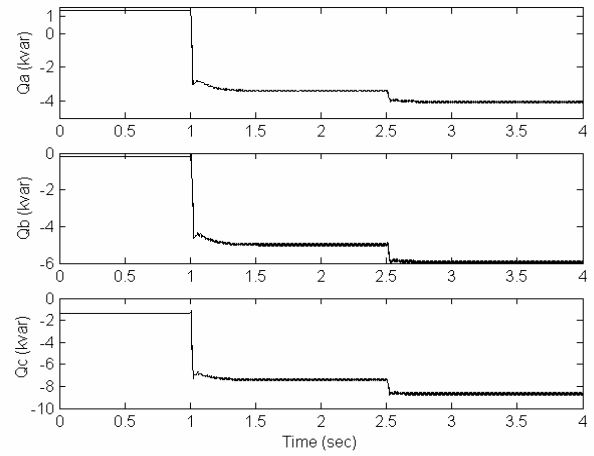


Fig. 8. Reactive power flow per phase of the inverter at node A (load convention).

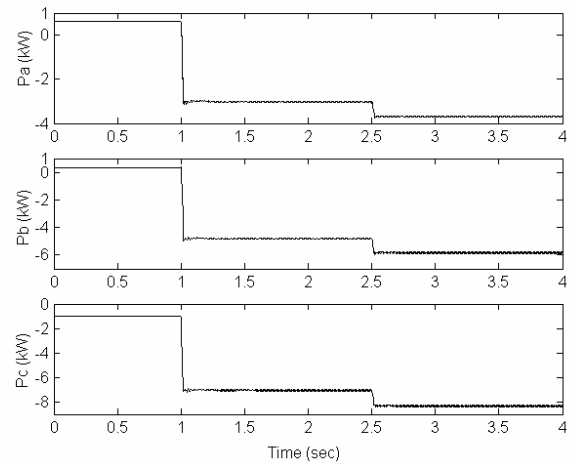


Fig. 9. Active power flow per phase of the inverter at node B (load convention).

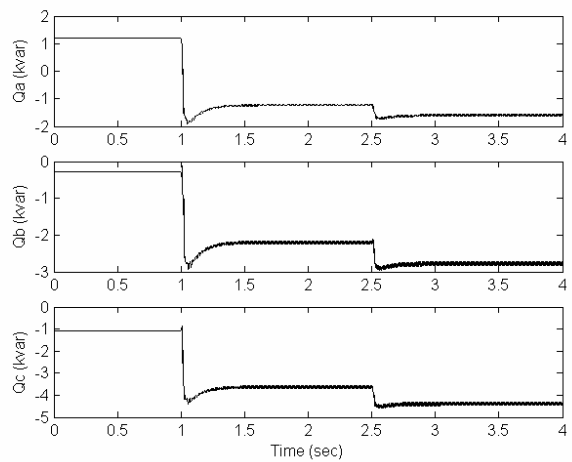


Fig. 10. Reactive power flow per phase of the inverter at node B (load convention).

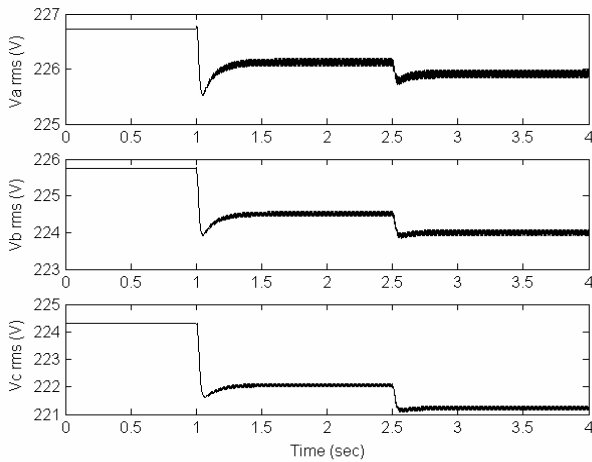


Fig. 11. Phase voltages at node C.

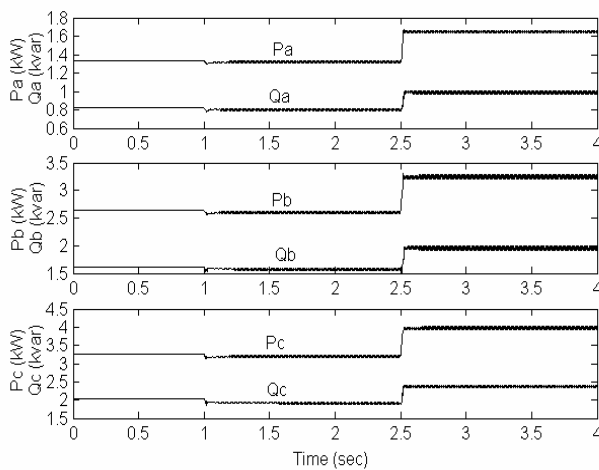


Fig. 12. P, Q flows per phase through the supply cable to node C (section 11 in Fig. 3).

For the second case studied, the same disturbance (isolation from the main grid) is simulated, but the two PV arrays and the WT of the micro-grid are now in operation from the beginning of the simulation. The PV units at nodes C and D produce 3 kW and 4 kW respectively, at unity power factor. The WT produces on average 5 kW and consumes 2.1 kvar. Its slip is  $-0.088$  and its input mechanical power 5.5 kW. To represent variations of the wind, a  $\pm 10\%$  periodic oscillation of frequency 0.5 Hz is superimposed on the average mechanical torque. The micro-grid is disconnected from the upstream network at 2.5 s and the output of the PV units is increased by 50% at 5 s, following an assumed increase in insolation. Selected waveforms are presented in Figs. 13 to 20.

Before the disconnection from the main grid, at  $t=2.5$  s, the micro-grid active load demand is covered only in part by the local production of the micro-sources, requiring a large power import from the upstream grid, which supplies the reactive power requirements, as well. Upon isolation, the two storage units start increasing their outputs to compensate the loss of the grid import (Fig. 17,18 for the storage unit at node B) and the micro-grid frequency drops to a lower value (Fig. 13). The active power production of the two PV units is increased by 50% at  $t=5$  s (Fig. 14 for the PV unit at node C), causing a

corresponding reduction in the active power production of the two storage units (Fig. 17) and a small increase in the frequency (Fig. 13). The changes of the aggregate (load and PV) powers and currents to node C are shown in Figs. 16 and 15. The active and reactive power and the rotor speed of the WT are presented in Figs. 19 and 20. Notably, the wind power fluctuations are also reflected on the system frequency and on the production of the battery inverters during the isolated mode of operation.

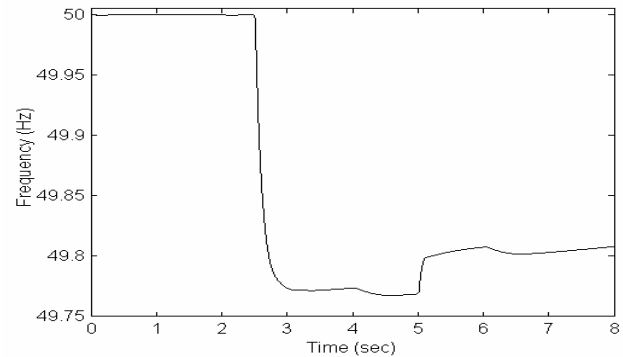


Fig. 13. Micro-grid frequency (measured at the terminals of the two battery units).

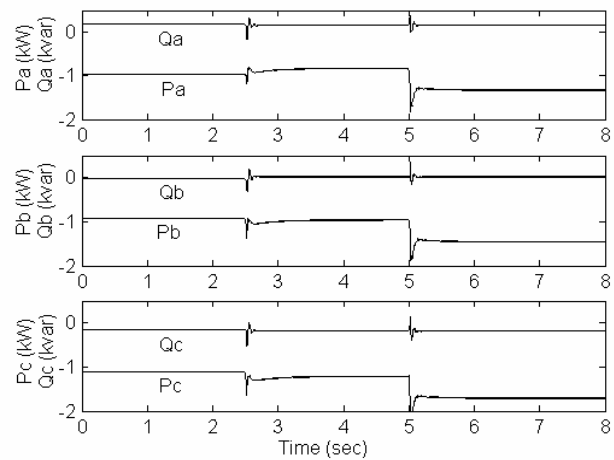


Fig. 14. P, Q output per phase of the PV inverter at node C (load convention).

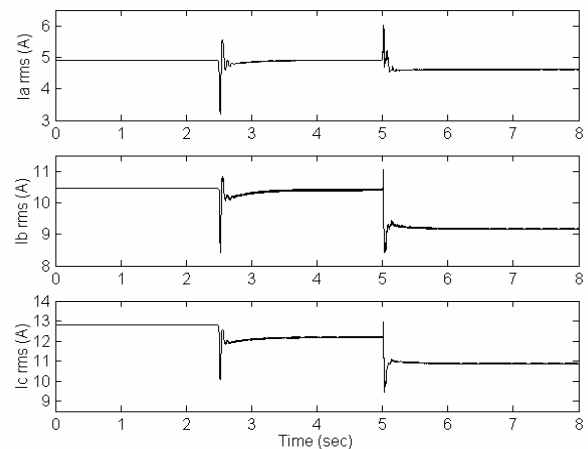


Fig. 15. Currents through the supply cable to node C (section 11 in Fig. 3).

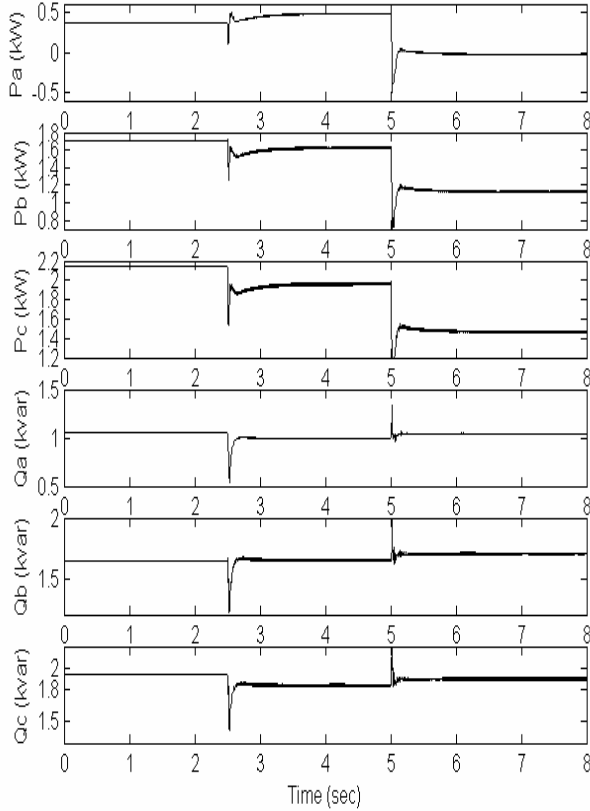


Fig. 16. P, Q per phase through the supply cable to node C (section 11 in Fig. 3).

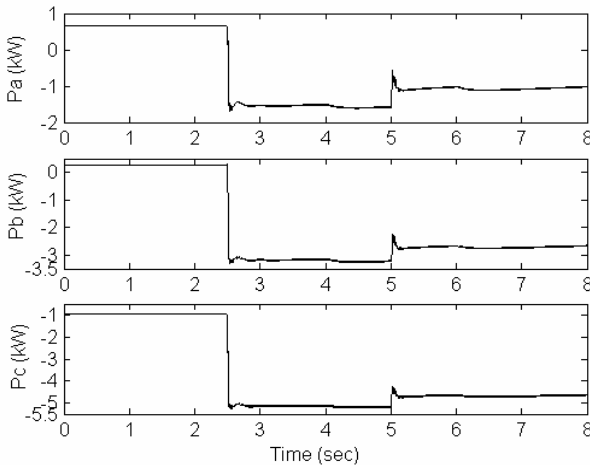


Fig. 17. Active power flow per phase of the inverter at node B (load convention).

#### IV. CONCLUSIONS

Simulation of an inverter dominated LV micro-grid using EMTP-RV was presented. Test cases demonstrated, include both grid-interconnected and isolated mode of operation. Particular characteristics of LV networks, such as network, load and source unbalances and neutral conductors, are accounted for in the system representation. The disturbances considered include sudden isolation from the upstream grid,

load changes and variations in the production of the micro-sources.

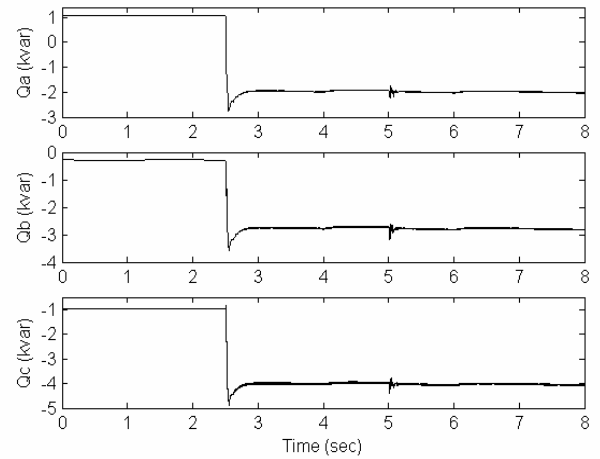


Fig. 18. Reactive power flow per phase of the inverter at node B (load convention).

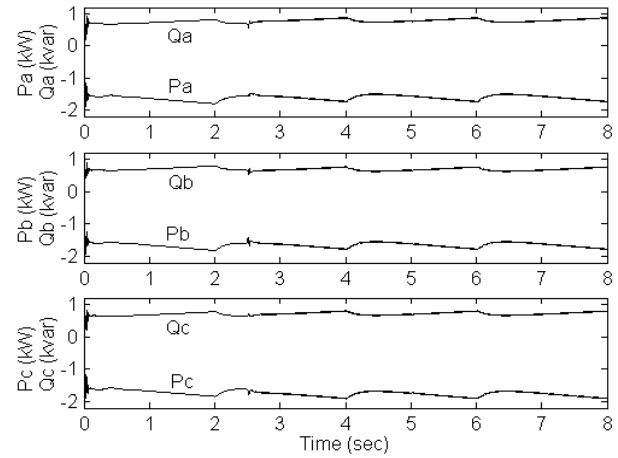


Fig. 19. P, Q output of the WT induction generator (load convention).

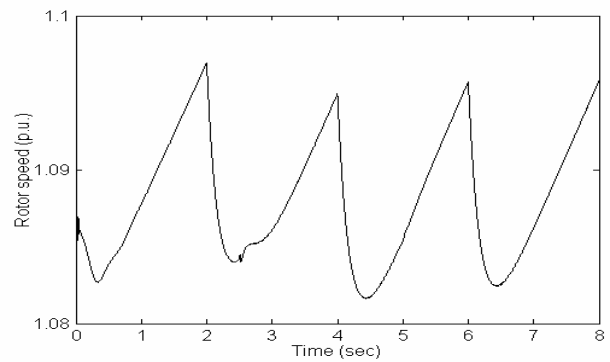


Fig. 20. Rotor speed of the WT.

#### V. APPENDIX

The output filter reactance of each inverter is 0.04 p.u. on its rating (lines 7, 12 in Fig. 3).

Control parameters (Fig. 1) for the storage unit inverters (on base power 100 kVA/phase):

	Unit at node A	Unit at node B
Slope of f-P droop curve (Hz/p.u. P)	-1.68	-2.353
Slope of V-Q droop curve (p.u. V/p.u. Q)	0.04	0.056
$T_m$	0.1 s	
$T_e$	0.08 s	

A value of ten times less the value of the f-P droop was used for the stabilizing gain of each unit.

Control parameters for the PV inverters (Fig. 2):

$$k_1 = 20, k_2 = 10, k_3 = 1400, C = 10 \text{ mF}, V_{dc-ref} = 1.4 \text{ pu}$$

WT induction generator parameters:

$$R_s = 2.52 \Omega, R_r = 2.67 \Omega, X_{ls} = X_{lr} = 3.39 \Omega, X_m = 197 \Omega$$

$$J = 0.486 \text{ Kg m}^2, 4 \text{ poles}$$

Table I provides data for the lines of the study case network of Fig. 3 (sequence quantities for compactness), derived by computing the 4x4 primitive impedance matrix of each cable type [17], based on the cables characteristics. For the single-phase line section 9 of Fig. 3, the actual loop impedance value is given.

TABLE I  
LINE DATA OF THE MICRO-GRID NETWORK

Line No	Line Type	$Z_{11}$ ( $\Omega/\text{km}$ )	$Z_{00}$ ( $\Omega/\text{km}$ )	Length (m)
1	Overhead – Bundled cable 4x120mm <sup>2</sup> AL XLPE	0.284 + j 0.0825	1.136 + j 0.417	35
2, 5, 8, 10	Overhead – Bundled cable 4x120mm <sup>2</sup> AL XLPE	0.284 + j 0.0825	1.136 + j 0.417	70
4	Overhead – Twisted cable 3x70mm <sup>2</sup> AL XLPE + 54.6mm <sup>2</sup> AAAC	0.497 + j 0.0861	2.387 + j 0.447	105
	Connection cable XLPE 3x50mm <sup>2</sup> AL + CU 35mm <sup>2</sup>	0.462 + j 0.0764	2.04 + j 0.421	30
6	Connection cable 4x25mm <sup>2</sup> CU	0.87 + j 0.0805	3.48 + j 0.409	20
9	Connection cable 2x6mm <sup>2</sup> CU	6.82 + j 0.192		20
11	Connection cable 4x16mm <sup>2</sup> CU	1.38 + j 0.0828	5.52 + j 0.418	30
3, 13	Connection cable 4x6mm <sup>2</sup> CU	3.41 + j 0.0963	13.64 + j 0.472	10

## VI. REFERENCES

- [1] R. Lasseter, A. Akhil, C. Marnay, J. Stephens, J. Dagle, R. Guttromson, A. Melliopoulos, R. Yinger, J. Eto, "White paper on integration of distributed energy resources - The CERTS micro-grid concept" Office of Power Technologies of the US Department of Energy, Contract, DE-AC03-76SF00098, April 2002.
- [2] "MICRO-GRIDS – Large Scale Integration of Micro-Generation to Low Voltage Grids", EU Contract ENK5-CT-2002-00610, Technical Annex, May 2002, also at <http://micro-grids.power.ece.ntua.gr>
- [3] Technical Brochure CIGRE Task Force 38.01.10, "Modeling new forms of generation and storage" Nov. 2000

- [4] N. Hatziaargyriou, G. Kariniotakis, N. Jenkins, J. Pecos Lopes, J. Oyarzabal "Modeling of Microsources for security studies", CIGRE Paris 30 Aug. – 3 Sep. 2004.
- [5] J. Mahseredjian, S. Denetiere, L. Dube, B. Khodabakhchian, L. Gerin-Lajoie, "On a new approach for the simulation of transients in power systems" presented at the *IPST '05 International Conference*, Montreal Canada, June 2005.
- [6] J. Mahseredjian, L. Dube, M. Zou, S. Denetiere, G. Joos, "Elimination of numerical delays in the solution of control systems in EMTF" presented at the *IPST '05 International Conference*, Montreal Canada, June 2005.
- [7] N. L. Soutanis, S. A. Papathanasiou, N. D. Hatziaargyriou, "A Stability Algorithm for the Dynamic Analysis of Inverter Dominated Unbalanced LV Microgrids.", *IEEE Transactions on Power Systems*, Volume 22, Issue 1, Feb. 2007, pp. 294 - 304
- [8] E. Clarke, *Circuit Analysis of A-C Power Systems*, vol. I. New York: Wiley, 1964
- [9] A. Engler, "Control of battery inverters in modular and expandable island grids." (In German), PhD dissertation, Univ. Kassel, Germany 2001.
- [10] A. Engler, "Applicability of droops in low voltage grids." *DER Journal* No 1, Jan. 2005.
- [11] S. Barsali, M. Ceraolo, P. Pelacchi, D. Poli, "Control techniques of dispersed generators to improve the continuity of electricity supply" in *Proc. 2002 IEEE Power Engineering Society Winter Meeting*, Vol. 2, pp. 27-32, Jan. 2002.
- [12] D. Georgakis, S. Papathanasiou, N. Hatziaargyriou, A. Engler, C. Hardt. "Operation of a prototype Micro-grid system based on micro sources equipped with fast-acting power electronics interfaces". *Proceedings of PESC'04*, June 2004, Aachen, Germany
- [13] M. C. Chandorkar, D. M. Divan, R. Adapa, "Control of parallel connected Inverters in stand alone AC supply systems", *IEEE Trans. Ind. Applications*, pp 136-143, Jan. 1993.
- [14] M. C. Chandorkar, D. M. Divan, B. Banerjee, "Control of distributed UPS systems", *Power Electronics Specialists Conference PESC' 94, 25<sup>th</sup> Annual IEEE*, Vol. 1, pp 197-204, June 1994.
- [15] O. Wasynczuk, N. A. Anwah, "Modeling and dynamic performance of a self commutated photovoltaic inverter system" *IEEE Trans. Energy Conversion* Vol. 4, No 3, pp 322-328, Sep. 1989.
- [16] S. Papathanasiou, N. Hatziaargyriou, K. Strunz, "A Benchmark Low Voltage Micro-grid Network" *Proc. CIGRE Symposium "Power Systems with Dispersed Generation"*, Athens, April 2005.
- [17] J. D. Glover, M. Sarma, *Power System Analysis & Design* PWS-Publishing 1994

## VII. BIOGRAPHIES

**Nikos L. Soutanis** received the Diploma in Electrical Engineering from NTUA in 1989 and the M.Sc. degree from UMIST Manchester, UK in 2000. Presently he is a PhD student in NTUA. His research interests are dispersed generation and power system analysis. He is a member of the IEE and of the Technical Chamber of Greece.

**A. I. Tsochnikas** received his Electrical and Computer Engineering degree at National Technical University of Athens (NTUA), in 2004. Currently he is a PhD student in the Electrical Engineering Department of NTUA. His research interests include renewable energy sources and dispersed generation.

**Nikos D. Hatziaargyriou** was born in Athens, Greece. He received the Diploma in Electrical and Mechanical Engineering from NTUA and the MSc and PhD degrees from UMIST, Manchester, UK. He is professor at the Power Division of the Electrical and Computer Engineering Department of NTUA. His research interests include Dispersed and Renewable Generation, Dynamic Security Assessment, and application of Artificial Intelligence Techniques to power systems. He is senior member of IEEE, member of CIGRE SCC6 and the Technical Chamber of Greece.

**Jean Mahseredjian** (M'87) graduated from École Polytechnique de Montréal with a Ph.D. in 1991. From 1987 to 2004 he worked at IREQ (Hydro-Québec) on research and development activities related to the simulation and analysis of electromagnetic transients. In December 2004 he joined the faculty of electrical engineering at École Polytechnique de Montréal.